Available online at www.sciencedirect.com
SCIENCE DIRECT
Thermochimica Acta 444 (2006) 166–172
thermochimica acta
www.elsevier.com/locate/tca

# Solid–liquid equilibria and purity determination for binary *n*-alkane + naphthalene systems

Kamel Khimeche [a,b], Yacine Boumrah [a], Mokhtar Benziane [a], Abdallah Dahmani [b,*]

[a] *Ecole Militaire Polytechnique EMP, BP 17 Bordj–el-Bahri, Alger, Algeria*
[b] *Laboratoire de Thermodynamique et de Modélisation Moléculaire, Faculté de Chimie, USTHB, BP. 32 El-Alia, 16111 Bab-Ezzouar, Alger, Algeria*

Received 27 December 2005; received in revised form 7 March 2006; accepted 7 March 2006
Available online 14 March 2006

**Abstract**

Mixtures of heavy aromatics with high aliphatics are important in the formation of asphaltenes in the oil industry.

This work reports binary solid–liquid equilibria for naphtalene + eicosane, +pentacosane, +hexatriacontane mixtures by differential scanning calorimetry. Results are compared with those from modified UNIFAC (Larsen and Gmehling versions) and ideal predictions. Finally, we determine the purity according to van't Hoff equation. Results are in good agreement with values given by ultraviolet spectrophotometry.
© 2006 Elsevier B.V. All rights reserved.

*Keywords:* DSC; Solid–liquid equilibria; *n*-Alkanes; Naphthalene; UNIFAC

## 1. Introduction

Solid –liquid phase equilibria form the basis for crystallization processes, which are used in chemical and petrochemical industry for separation of mixtures. Mixtures of high normal long-chain alkanes and polyaromatics are important in the flocculation of asphaltenes, and their codeposition constitutes a major problem during the exploitation, transport, and storage of crude oil.

The experimental determination of thermodynamic and structural properties of pure long-chain *n*-alkanes and phase diagrams of their molecular alloys have been the subject of many investigations in the literature [1–10]. Some data concerning solid–liquid equilibria of normal long-chain alkanes + organic compounds have been reported [11–17].

Following a systematic study of the thermodynamic properties of mixtures containing organic molecules [18,19], we present in this paper data on solid–liquid equilibria (SLE) of naphthalene + eicosane, +pentacosane, +hexatriacontane systems which represent a particularly interesting family of molecules for testing theories and can be helpful to understand the phase behavior of heavy oils. Results obtained are compared with those given by modified UNIFAC (Larsen and Gmehling versions) and ideal models [20,21]. The experimental results were also exploited in the determination of purity [22–25].

## 2. Experimental procedures

### 2.1. Materials and methods

Naphthalene, *n*-eicosane, *n*-pentacosane and *n*-hexatriacontane were purchased from Fluka (purity greater than 99 mol%) and by gas chromatography have a purity >99.5%. They were used without further purification.

A series of heavy alkane–naphthalene binary mixtures were prepared by heating very slowly in a glass cell near the melting temperature of the major component.

With continuous stirring, the liquefied sample was quenched in liquid nitrogen, ground and powdered in a clean agate mortar with as little pressure as possible (the crystal lattice of some substances can be destroyed by excessive pressure) and dried in a desiccator. The rapid cooling of molten samples ensured a uniform steric concentration of components in the mixture and homogeneity of the final molecular alloy [3].

For the analysis, 1–8 mg of solid was sealed in a DSC 7 Perkin–Elmer pan. The measurements were carried out at constant heating rate of 1 K $min^{-1}$ under nitrogen atmosphere (20 ml $min^{-1}$). For purity determination, 1–2 mg accurately

* Corresponding author. Tel.: +213 62 12 99 93; fax: +213 21 24 73 11.
*E-mail address:* abdahmani@yahoo.fr (A. Dahmani).

0040-6031/$ – see front matter © 2006 Elsevier B.V. All rights reserved.
doi:10.1016/j.tca.2006.03.011

weighed samples were run at a scanning rate of $1\,K\,min^{-1}$ [23,25]. Prior to the analysis, the DSC7 was calibrated with indium 99.999% (supplied by Perkin–Elmer), melting point 156.60 °C and enthalpy of fusion $28.45\,J\,g^{-1}$. Data acquisition (enthalpy of fusion of the pure compounds and onsets of the solid–liquid equilibria temperatures) and processing was done with Perkin–Elmer's Pyris software. The uncertainties of the measurements are estimated to be ±0.1 K for the temperatures and $\pm 0.20\,kJ\,mol^{-1}$ for the heats of fusion and solid–solid transition. The masses of the samples were determined with a precision ±0.2 mg with a Mettler H31 balance. The uncertainty of mole fraction did not exceed 0.0005.

For purity determination, the mixtures were also subjected to UV spectrophotometry (Helios Beta). Maximum absorption was at 275 nm for naphthalene and eicosane in 95% (v/v) ethanol and for naphthalene, pentacosane and hexatriacontane in tetrahydrofuran.

A series of solutions prepared with these components and their mixtures were measured at 275 nm for different concentrations to construct a calibration curve with ethanol or THF as a blank.

## 3. Results and discussion

### 3.1. Solid–liquid equilibria

Typical DSC curves obtained are shown in Figs. 1–3. The thermodynamic properties of the pure compounds (Table 1) are in good agreement with literature data [1,11,26–31]. Tables 2–4 list the experimental results of each system. Plots of the eutectic heat $\Delta H_e$ and fusion heat $\Delta H_m$ versus naphthalene mole fractions (Figs. 4–6) illustrate that naphthalene (1) + *n*-eicosane (2), naphthalene (1) + *n*-pentacosane (2) and naphthalene (1) + *n*-hexatriacontane (2) mixtures form single eutectics corresponding respectively for naphthalene molar fractions: $x_1 = 0.349$, 0.450, 0.751 and temperatures of 308.3, 318.6 and 339.4 K.

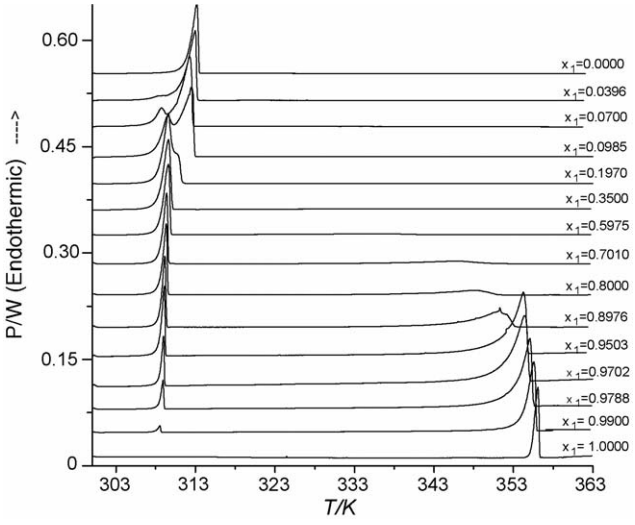


Fig. 1. DSC curves for naphthalene (1) + *n*-eicosane (2) mixtures.

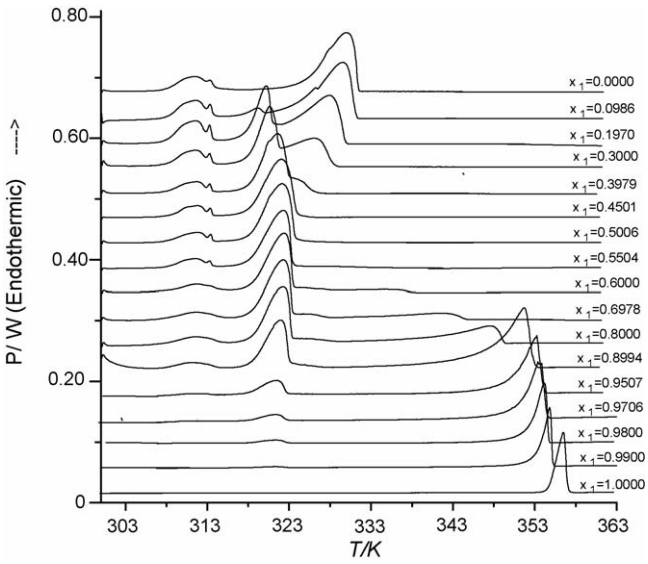


Fig. 2. DSC curves for naphthalene (1) + *n*-pentacosane (2) mixtures.

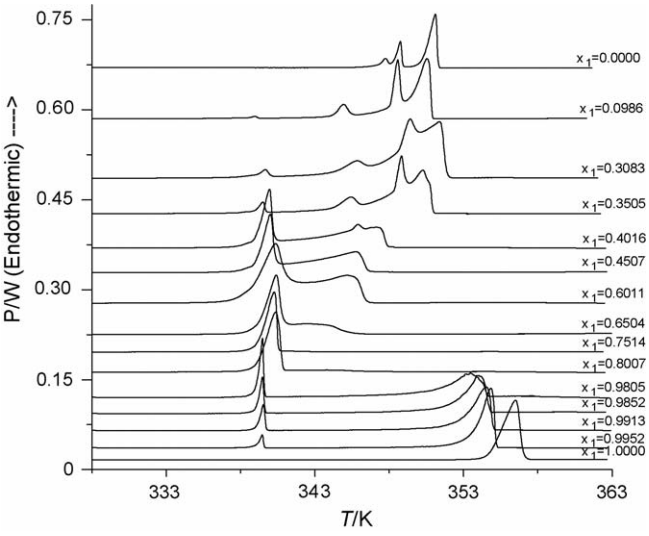


Fig. 3. DSC curves for naphthalene (1) + *n*-hexatriacontane (2) mixtures.

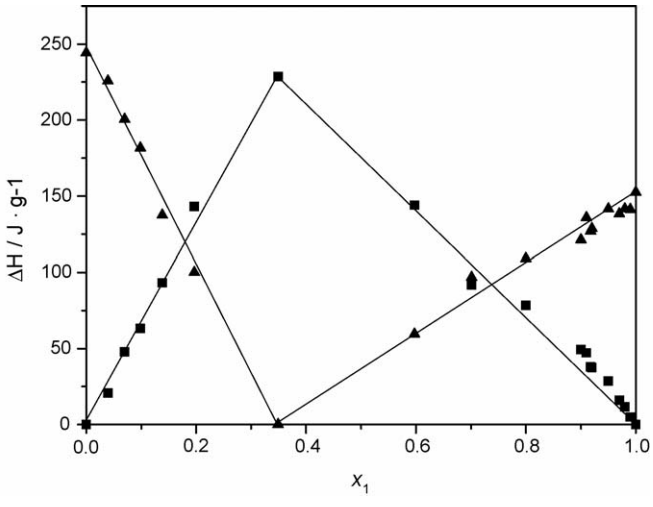


Fig. 4. The eutectic heat $\Delta H_e$ (■) and heat of melting $\Delta H_m$ (▲) for different compositions for the mixture naphthalene (1) + eicosane (2).

Table 1
Thermodynamic properties of pure compounds

| Compound | $T_m$ (K) | $\Delta H_m$ (kJ mol$^{-1}$) | $T_{tr}$ (K) | $\Delta H_{tr}$/kJ mol$^{-1}$ |
|---|---|---|---|---|
| Eicosane | 311.60[a] | 69.03[a] | | |
| | 309.50[b] | 69.73[b] | | |
| | 310.00[c] | 69.88[c] | | |
| | 309.75[d] | | | |
| | 309.70[e] | | | |
| Pentacosane | 325.92[a] | 55.53[a] | 309.00[a]; 312.90[a] | 23.90[a]; 1.07[a] |
| | 326.30[b] | 57.09[b] | 320.3[b] | 26.67[b] |
| | 326.00[c] | 54.04[c] | 319.30[c] | 24.43[c] |
| | 326.90[e] | 57.78[e] | 320.00[f]; 320.15[f] | 26.08[f] |
| | 326.65[f] | 56.58[f] | 320.0[g]; 310.50[g]; 319.40[g] | |
| | | | 321.20[g]; 322.60[g]. | |
| Hexatriacontane | 350.19[a] | 81.55[a] | 347.33[a]; 348.28[a] | 11.73[a]; 24.72[a] |
| | 348.95[b] | 87.68[b] | 347[b] | 31.07[b] |
| | 348.80[c] | 91.33[c] | 345.05[d]; 345.35[d] | 9.90[d]; 30.51[d] |
| | 349.15[d] | 88.74[d] | 345.25[f]; 346.95[f] | 9.91[f]; 30.54[f] |
| | 349.05[f] | 88.83[f] | 345.39[i]; 346.83[i] | 10.09[i]; 32.12[i] |
| | 348.94[i] | 87.68[i] | | |
| Naphthalene | 354.69[a] | 19.55[a] | | |
| | 353.4[h] | 18.24[h] | | |

[a] Our experimental values.
[b] Ref. [5].
[c] Ref. [15].
[d] Ref. [30].
[e] Ref. [31].
[f] Ref. [32].
[g] Ref. [33].
[h] Ref. [34].
[i] Ref. [35].

The DSC curves show that naphthalene + $n$-$C_{25}$ and naphthalene + $n$-$C_{36}$ exhibit solid–solid transitions. For the system naphthalene + $n$-$C_{25}$, the temperatures corresponding to solid–solid transitions are different from those given by literature [1,11,28,29]. According to Robles et al. [29], the molecules of $n$-alkanes from $C_{22}H_{46}$ to $C_{27}H_{56}$ are always parallel, their end methyl groups forming parallel layers. At low temperature ordered crystalline forms are observed and their nature depends on the parity of n the number of carbon atoms. Thus the first transition ($T_{tr1}$ = 309.0 K, $\Delta H_{tr1}$ = 23.90 kJ mol$^{-1}$) is attributed to the passage from an ordered orthorhombic β phase to an orthorhombic solid β′ phase. The second transition ($T_{tr2}$ = 312.9 K, $\Delta H_{tr2}$ = 1.07 kJ mol$^{-1}$) is attributed to an allotropic transformation of an ordered low temperature β′ phase to an ordered monoclinic solid phase M*.

The second system exhibits two solid–solid transitions for $x_1 \leq 0.450$.

According to the literature [28,32], $C_{36}H_{74}$ displays monoclinic and orthorhombic phases, which depend on the thermal treatment and purity. The transition ($T_{tr1}$ = 347.3 K, $\Delta H_{tr1}$ = 11.73 kJ mol$^{-1}$) is attributed to the transformation from low temperature monoclinic form ($M_L$) into the high-

Table 2
Experimental solid–liquid equilibrium temperature for the system naphthalene (1) + $n$-$C_{20}$ (2)

| $x_1$ | $T_2$ (K) | $T_1$ (K) | $x_1$ | $T_1$ (K) |
|---|---|---|---|---|
| 0.000 | 311.6 | | 0.597 | 330.4 |
| 0.019 | 311.5 | | 0.650 | 333.9 |
| 0.039 | 311.2 | | 0.701 | 338.7 |
| 0.070 | 310.7 | | 0.800 | 342.4 |
| 0.098 | 310.6 | | 0.897 | 347.7 |
| 0.197 | 310.4 | | 0.910 | 349.2 |
| 0.250 | 309.7 | | 0.917 | 349.4 |
| 0.298 | 308.8 | | 0.920 | 349.5 |
| 0.349 | | 308.3 | 0.950 | 351.6 |
| 0.400 | | 312.7 | 0.970 | 352.1 |
| 0.450 | | 317.2 | 0.978 | 353.4 |
| 0.501 | | 322.5 | 0.990 | 354.1 |
| 0.540 | | 325.6 | 1.000 | 354.7 |

Table 3
Experimental solid–liquid equilibrium temperature for the system naphthalene (1) + $n$-$C_{25}$ (2)

| $x_1$ | $T_2$ (K) | $T_1$ (K) | $x_1$ | $T_1$ (K) |
|---|---|---|---|---|
| 0.000 | 325.9 | | 0.648 | 331.6 |
| 0.050 | 325.6 | | 0.698 | 333.5 |
| 0.098 | 323.8 | | 0.744 | 337.2 |
| 0.197 | 323.0 | | 0.800 | 341.5 |
| 0.300 | 321.5 | | 0.899 | 347.3 |
| 0.398 | 319.7 | | 0.951 | 350.4 |
| 0.450 | 318.6 | | 0.971 | 351.4 |
| 0.501 | | 322.7 | 0.980 | 352.7 |
| 0.550 | | 325.1 | 0.990 | 353.5 |
| 0.600 | | 327.4 | 1.000 | 354.7 |

Table 4
Experimental solid–liquid equilibrium temperature for the system naphthalene (1) + $n$-$C_{36}$ (2)

| $x_1$ | $T_{\alpha 2}$ (K) | $T_{\beta 2}$ (K) | $T_{\gamma 2}$ (K) | $x_1$ | $T_1$ (K) |
|---|---|---|---|---|---|
| 0.000 | 350.2 | | | 0.751 | 339.4 |
| 0.099 | 350.0 | | | 0.801 | 342.2 |
| 0.200 | 349.4 | | | 0.852 | 345.3 |
| 0.308 | 348.5 | | | 0.900 | 347.8 |
| 0.350 | | 347.9 | | 0.971 | 350.9 |
| 0.401 | | 346.4 | | 0.981 | 351.3 |
| 0.451 | | | 344.3 | 0.985 | 352.5 |
| 0.550 | | | 343.6 | 0.991 | 352.9 |
| 0.601 | | | 343.3 | 0.995 | 353.6 |
| 0.650 | | | 342.1 | 1.000 | 354.7 |
| 0.700 | | | 341.5 | | |

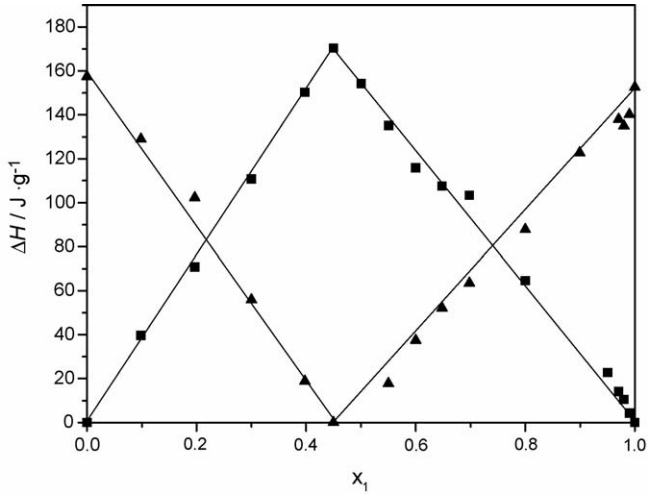


Fig. 5. The eutectic heat $\Delta H_e$ (■) and heat of melting $\Delta H_m$ (▲) for different compositions for the mixture naphthalene (1) + $n$-pentacosane (2).

temperature monoclinic form ($M_H$). The second transition ($T_{tr2}$ = 348.3 K, $\Delta H_{tr2}$ = 24.72 kJ mol$^{-1}$) is probably the passage from the monoclinic ($M_H$) phase to the rotator phase (R). The temperatures, about (348.18 K) and (349.27 K), correspond to

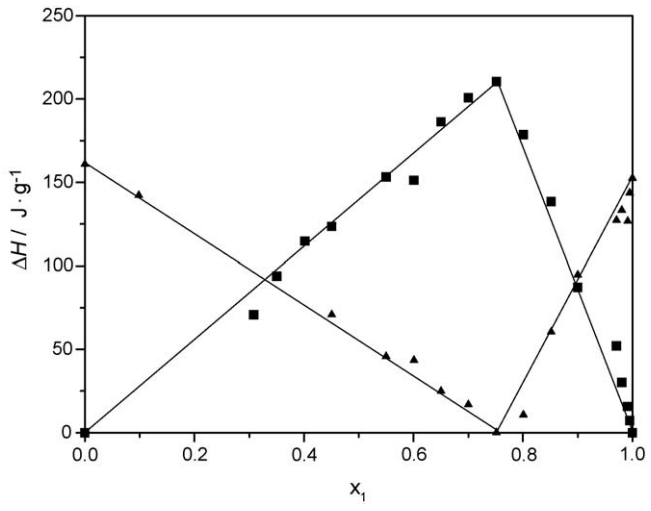


Fig. 6. The eutectic heat $\Delta H_e$ (■) and heat of melting $\Delta H_m$ (▲) for different compositions for the mixture naphthalene (1) + $n$-hexatriacontane (2).

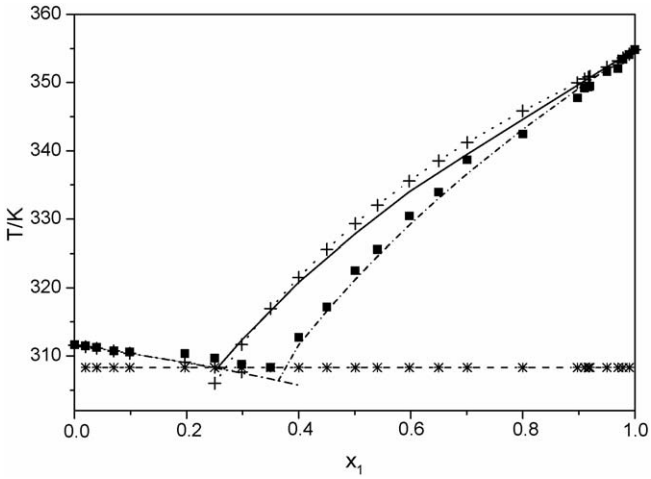


Fig. 7. Experimental and predicted SLE phase diagrams of naphthalene (1) + $n$-eicosane (2) mixture: (■), experimental results; (—), modified UNIFAC (Larsen) model; (· · ·+· · ·), modified UNIFAC (Gmehling) model; (–·–·–·–), ideal model; (-✳-), eutectic temperature.

the end of the ($M_L$)–($M_H$) phase transition and the ($M_H$)–(R) rotator phase transition, respectively.

The polymorphism observed in $n$-alkanes has been reviewed in detail [1,3,4,32–36].

SLE data can be used to calculate activity coefficients of the mixture components. In the case of the systems studied, the components are not miscible in the solid phase and all diagrams present a simple eutectic. Therefore, the activity coefficient $\gamma_i$ of the component $i$, in the liquid phase can be calculated according to the following expression [12,37–39]:

$$\ln x_i\gamma_i = -\frac{\Delta H_{m,i}}{RT}\left(1-\frac{T}{T_{m,i}}\right)+\frac{\Delta C_{p,i}}{R} \times\left(\ln\frac{T}{T_{m,i}}+\frac{T_{m,i}}{T}-1\right)-\frac{\Delta H_{tr,i}}{RT}\left(1-\frac{T}{T_{tr,i}}\right), \quad (1)$$

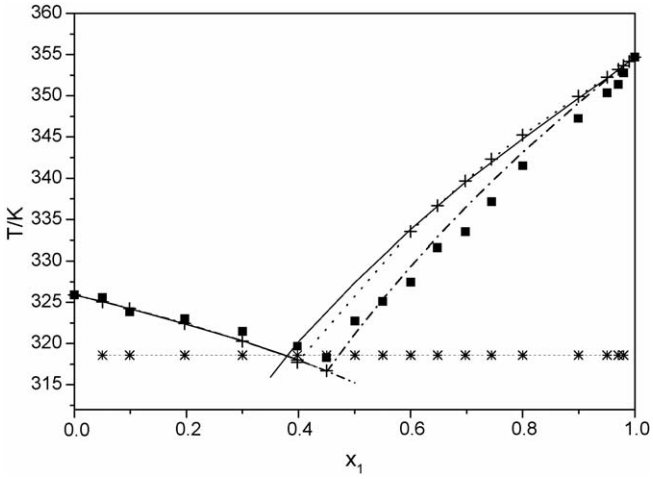


Fig. 8. Experimental and predicted SLE phase diagrams of naphthalene (1) + $n$-pentacosane (2) mixture: (■), experimental results; (—), modified UNIFAC (Larsen) model; (· · ·+· · ·), modified UNIFAC (Gmehling) model; (–·–·–·–), ideal model; (-✳-), eutectic temperature.

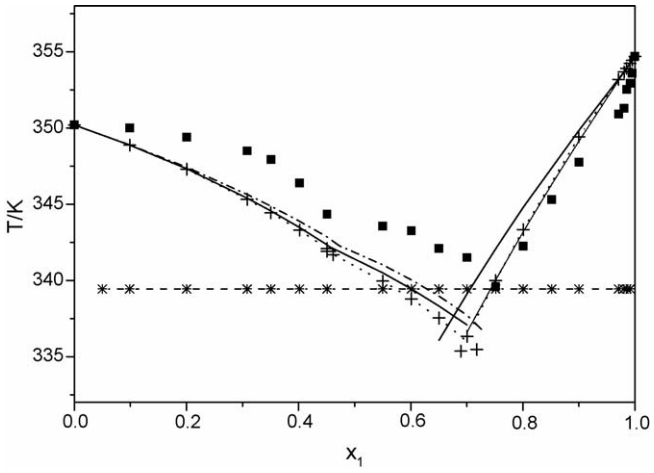


Fig. 9. Experimental and predicted SLE phase diagrams of naphthalene (1) + *n*-hexatriacontane (2) mixture: (■), experimental results; (—), modified UNIFAC (Larsen) model; (· · ·+· · ·), modified UNIFAC (Gmehling) model; (—·—·—), ideal model; (⁎), eutectic temperature.

Table 5
Values of the relative standard deviations, $\sigma$[a] and of absolute mean deviations, $\Delta$[b] of the equilibrium temperature calculated by UNIFAC (Larsen and Gmehling versions) and ideal models, $N$ is the number of data points

| System | $N$ | Larsen | | Gmehling | | Ideal | |
|---|---|---|---|---|---|---|---|
| | | $\Delta T$ (K) | $\sigma$ | $\Delta T$ (K) | $\sigma$ | $\Delta T$ (K) | $\sigma$ |
| Naphthalene (1) + *n*-$C_{20}$ (2) | 26 | 1.7 | 0.011 | 1.9 | 0.013 | 0.6 | 0.017 |
| Naphthalene (1) + *n*-$C_{25}$ (2) | 20 | 1.9 | 0.011 | 1.7 | 0.010 | 0.4 | 0.012 |
| Naphthalene (1) + *n*-$C_{36}$ (2) | 21 | 2.9 | 0.010 | 2.4 | 0.014 | 1.7 | 0.006 |

[a] $\sigma = \left[\frac{1}{N}\sum_{i=1}^{N}\left(\frac{T_{i\,\mathrm{cal}}-T_{i\,\mathrm{exp}}}{T_{i\,\mathrm{exp}}}\right)^2\right]^{1/2}$.

[b] $\Delta T\,(\mathrm{K}) = \frac{1}{N}\sum_{i=1}^{N}|T_{i\,\mathrm{cal}} - T_{i\,\mathrm{exp}}|$.

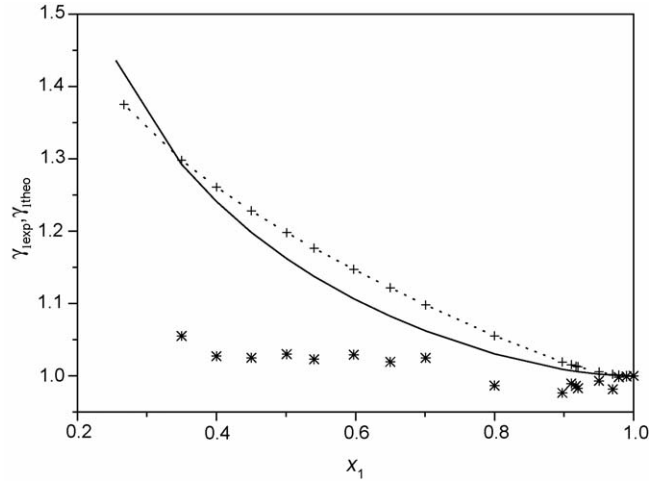


Fig. 10. Experimental and predicted activity coefficient, $\gamma_1$, vs. $x_1$ for naphthalene (1) + *n*-eicosane (2) mixture: (⁎), experimental results; (—), modified UNIFAC (Larsen); (· · ·+· · ·), modified UNIFAC (Gmehling).

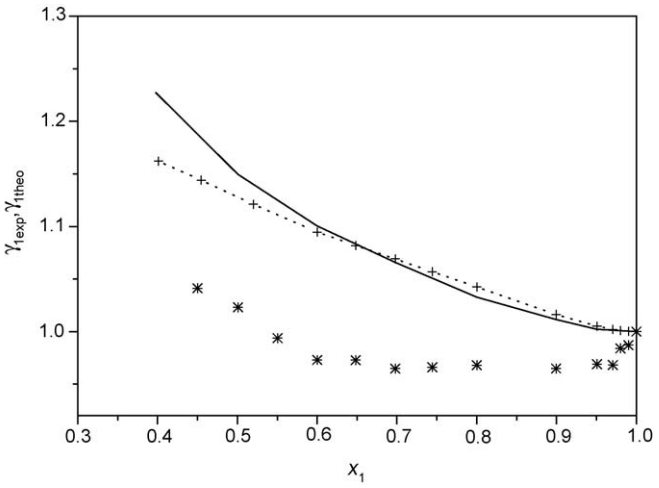


Fig. 11. Experimental and predicted activity coefficient, $\gamma_1$, vs. $x_1$ for naphthalene (1) + *n*-pentacosane (2) mixture: (⁎), experimental results; (—), modified UNIFAC (Larsen); (· · ·+· · ·), modified UNIFAC (Gmehling).

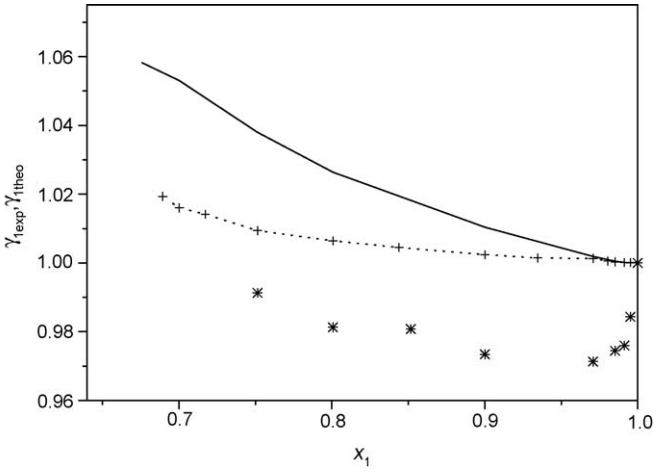


Fig. 12. Experimental and predicted activity coefficient, $\gamma_1$, vs. $x_1$ for naphthalene (1) + *n*-hexatriacontane (2) mixture: (⁎), experimental results; (—), modified UNIFAC (Larsen); (· · ·+· · ·), modified UNIFAC (Gmehling).

Table 6
Comparison of experimental coordinates of eutectic points: $T_{eu}$ (K) and mole fraction, $x_{1eu}$ with values calculated by UNIFAC (Larsen and Gmehling versions) and ideal models

| System | $T_{eu}$ (K) | | $x_{1eu}$ | |
|---|---|---|---|---|
| | Exp. | Cal. | Exp. | Cal. |
| Naphthalene (1) + *n*-$C_{20}$ (2) | 308.3 | 308.26[a] | 0.35 | 0.256[a] |
| | | 307.92[b] | | 0.267[b] |
| | | 306.30[c] | | 0.363[c] |
| Naphthalene (1) + *n*-$C_{25}$ (2) | 318.6 | 318.41[a] | 0.45 | 0.379[a] |
| | | 317.84[b] | | 0.401[b] |
| | | 316.61[c] | | 0.449[c] |
| Naphthalene (1) + *n*-$C_{36}$ (2) | 339.4 | 337.64[a] | 0.75 | 0.676[a] |
| | | 336.09[b] | | 0.696[b] |
| | | 337.33[c] | | 0.711[c] |

[a] Calculated by UNIFAC (Larsen version).
[b] Calculated by UNIFAC (Gmehling version).
[c] Calculated (ideal model).

Table 7
Impurities determined from the van't Hoff plot and UV spectrophotometry[a] deviation = $[(x_1^{DSC} - x_1^{UV})/x_1^{UV}] \times 100$

| Major Component (1) | Impurity (2) | Expected ($x_2$) | $x_1^{UV}$: UV spectrophotometry method | $x_1^{DSC}$: The van't Hoff plot | Deviation (%) |
|---|---|---|---|---|---|
| Naphthalene | *n*-C20 | 0.01 | 0.9872 (0.0007) | 0.9889 (0.0019) | 0.17 |
| | | 0.02 | 0.9737 (0.0005) | 0.9751 (0.0014) | 0.14 |
| | | 0.03 | 0.9599 (0.0003) | 0.9712 (0.0010) | 1.18 |
| | | 0.05 | 0.9450 (0.0045) | 0.9661 (0.0009) | 2.23 |
| | | 0.08 | 0.9080 (0.0098) | 0.9447 (0.0007) | 4.04 |
| | *n*-C25 | 0.01 | 0.9863 (0.0033) | 0.9846 (0.0013) | −0.17 |
| | | 0.02 | 0.9812 (0.0055) | 0.9768 (0.0017) | −0.45 |
| | | 0.03 | 0.9465 (0.0010) | 0.9537 (0.0019) | 0.76 |
| | | 0.05 | 0.9398 (0.0087) | 0.9631 (0.0004) | 2.48 |
| | | 0.08 | 0.9046 (0.0013) | 0.9429 (0.0006) | 4.23 |
| | *n*-C36 | 0.01 | 0.9889 (0.0018) | 0.9897 (0.0013) | 0.08 |
| | | 0.02 | 0.9856 (0.0008) | 0.9756 (0.0015) | −1.01 |
| | | 0.03 | 0.9640 (0.0043) | 0.9684 (0.0008) | 0.46 |
| | | 0.05 | 0.9324 (0.0009) | 0.9623 (0.0017) | 3.21 |
| | | 0.08 | 0.9014 (0.0189) | 0.9325 (0.0007) | 3.45 |

[a] Values are mean (standard deviation) calculated from three replications.

where, $\Delta H_{m,i}$, $T_{m,i}$, $\Delta C_{p,i}$, $\Delta H_{tr,i}$ and $T_{tr,i}$, are respectively, the molar enthalpy of melting, melting temperature, molar heat capacity change (assumed to be independent of $T$) during the fusion process, enthalpy change corresponding to the transition and transition temperature of the pure component $i$. Because of the lack of appropriate data representing $\Delta C_{p,i}$ and considering its weak contribution, as cited in the literature [40], the related terms in Eq. (1) were neglected. The required physical constants of the pure compounds are reported in Table 1.

The modified UNIFAC, Larsen et al., and Gmehling et al. were used for the calculation of the activity coefficients and prediction of SLE. Values of the required geometrical and interaction parameters of our systems have been given elsewhere [41,42] and were used without modification. Experimental SLE phase diagrams are in good agreement with those obtained by UNIFAC and ideal thermodynamic models, as shown in Figs. 7–9. For the binary (naphthalene + *n*-alkanes), the relative and the absolute mean deviations of the equilibrium temperatures are given in Table 5. The deviations observed in the experimental and calculated activity coefficients of naphthalene $\gamma_1$ as illustrated by Figs. 10–12, can be attributed to the limits of application of the group contribution methods in the case of complex systems like polyaromatics + *n*-alkane mixtures. The difficulties in representing complex systems are not surprising because a simple group contribution method is not able to account for the order/disorder effect. The long-chain compounds are highly ordered in the solid state. In the liquid state they still retain much of their order [43]. The thermodynamic properties of *n*-alkanes + cyclic molecule mixtures are due essentially to the combinatorial, free volume and interactional contributions [44,45]. The importance of the combinatorial effect is examined in detail by Kniaz [43]. As shown in Table 6, the experimental values of $T_{eu}$ and $x_{1eu}$ corresponding to the eutectic points are close to those predicted by the different models and depend on the chain length of *n*-alkane. They increase with the increase of the number of carbon atoms of the *n*-alkanes.

### 3.2. DSC purity determination

An ideal solution may be approached in the melt of naphthalene doped with a very small amount of the *n*-alkane. This behavior is an important condition in the experimental purity determination by DSC.

Eutectic impurities lower the melting point of the eutectic system. This Effect is described by the van't Hoff equation:

$$T_{m,1} - T_m^* = \frac{T_{m,1}^2 x_2^*}{\Delta H_{m,1}} \times \frac{1}{F} \quad (2)$$

where $T_m^*$ is the melting temperature of the impure material (which, during melting, follows the liquidus temperature), $T_{m,1}$ and $\Delta H_{m,1}$ the melting point and the molar heat of melting (calculated from the peak area) of the pure substance 1, $R$ the gas constant, $F$ the fraction molten corresponding to $T_m^*$ and $x_2^*$ is the concentration (mole fraction of the impurity to be determined).

Purities obtained by DSC, using van't Hoff plots are in good agreement with results given by the UV spectrophotometric method. The values of naphthalene fraction ($x_1$) determined by the van't Hoff plot and the corresponding values determined by UV spectrophotometric methods are tabulated in Table 7.

The DSC method of purity determination may be limited to high-purity samples. This study observed that maximum concentration levels for van't Hoff law applicability could be as high as 3 mol% of the impurity.

## References

[1] M. Dirand, M. Bouroukba, A.J. Briard, V. Chevallier, D. Petitjean, J.P. Corriou, J. Chem. Thermodyn. 34 (2002) 1255–1277.
[2] A. Sabour, J.B. Bourdet, M. Bouroukba, M. Dirand, Thermochim. Acta 249 (1995) 269–283.
[3] V. Chevallier, D. Petitjean, V.R. Meray, M. Dirand, Polymer 40 (1999) 5953–5956.
[4] M. Dirand, Z.A. Boudjema, J. Mol. Struct. 375 (1996) 243–248.

[5] V. Chevalier, D. Petitjean, M. Bouroukba, M. Dirand, Polymer 40 (1999) 2129, 2137.
[6] H. Nouar, D. Petitjean, J.B. Bourdet, M. Bouroukba, M. Dirand, Thermochim. Acta 293 (1997) 87–92.
[7] D. Petitjean, M. Pierre, P. Goghomu, M. Bouroukba, M. Dirand, Polymer 43 (2002) 345–349.
[8] E. Provost, D. Balesdent, M. Bouroukba, D. Petitjean, M. Dirand, V.R. Meray, J. Chem. Thermodyn. 31 (1999) 1135–1150.
[9] Z.A. Boudjema, M. Bouroukba, M. Dirand, Thermochim. Acta 276 (1996) 243–256.
[10] V. Chevalier, E. Provost, J.B. Bourdet, M. Bouroukba, D. Petitjean, M. Dirand, Polymer 40 (1999) 2121–2128.
[11] R. Mahmoud, R. Solimando, M. Bouroukba, M. Rogalski, J. Chem. Eng. Data 45 (2000) 433–436.
[12] G. Chandra Sekhar, P. Venkatesu, T. Hofman, M.V. Prabhakara Rao, Fluid Phase Equilib. 201 (2002) 219–231.
[13] U. Domanska, M. Szurgocinska, J.A. Gonzalez, Fluid Phase Equilib. 190 (2001) 15–31.
[14] P. Morawski, J.A.P. Coutinho, U. Domanska, Fluid Phase Equilib. 230 (2005) 72–80.
[15] U. Domanska, P. Morawski, Fluid Phase Equilib. 218 (2004) 57–68.
[16] U. Domanska, J.A. Gonzalez, Fluid Phase Equilib. 147 (1998) 251–270.
[17] R. Mahmoud, R. Solimando, M. Rogalski, Fluid Phase Equilib. 148 (1998) 139–146.
[18] F. Allal, A. Dahmani, Fluid Phase Equilib. 190 (2001) 33–45.
[19] M. Benkhennouf, K. Khimeche, A. Dahmani, J. Phys. IV-France 113 (2004) 7–9.
[20] B.L. Larsen, P. Rasmussen, A. Frendeslund, Ind. Eng. Chem. Res. 26 (1987) 2274–2286.
[21] J. Gmehling, J. Li, M. Schiller, Ind. Eng. Chem. Res. 32 (1993) 178–193.
[22] K. Yoshii, Chem. Pharm. Bull. 45 (1997) 338–343.
[23] R.L. Blaine, C.K. Schoff (Eds.), Purity Determinations by Thermal Methods, ASTM, STP 834, American Society for Testing and Materials, 1984.
[24] H.E. Gallis, G.J.K. van den Berg, H.A.J. Oonk, J. Chem. Eng. Data 41 (1996) 1303–1306.
[25] N.J. De Angelis, G.J. Papariello, J. Pharm. Sci. 57 (1968) 1868–1873.
[26] J. Company, Chem. Eng. Sci. 28 (1973) 318–323.
[27] U. Domanska, J.A. Gonzalez, Fluid Phase Equilib. 147 (1998) 251–270.
[28] A.A. Schaerer, C.J. Busso, A.E. Smith, L.B. Skinner, J. Am. Chem. Soc. 77 (1955) 2017–2019.
[29] L. Robles, D. Mondieig, Y. Haget, M.A. Cuevas-Diarte, J. Chim. Phys. 95 (1998) 92–111.
[30] C. Peng, H. Liu, Y. Hu, Fluid Phase Equilib. 180 (2001) 299–311.
[31] L. Wang, Z.C. Tan, S.H. Meng, D.B. Liang, Thermochim. Acta 342 (1999) 59–65.
[32] H. Honda, H. Ogura, S. Tasaki, A. Chiba, Thermochim. Acta 405 (2003) 51–60.
[33] E.B. Sirota, H.E. King, D.M. Singer, H. Sao, J. Chem. Phys. 98 (1993) 5809–5816.
[34] E.B. Sirota, D.M. Singer, J. Chem. Phys. 101 (1994) 10873–10881.
[35] P.S. Bagus, K. Weiss, A. Schertel, C. Wöll, W. Braun, C. Hellwig, C. Jung, Chem. Phys. Lett. 248 (1996) 129–135.
[36] S.Y. Chazhengina, E.N. Kotelnikova, I.V. Filippova, S.K. Filatov, J. Mol. Struct. 647 (2003) 243–257.
[37] A. Jakob, R. Joh, C. Rose, J. Gmehling, Fluid Phase Equilib. 113 (1995) 117–126.
[38] U. Domanska, J.A. Gonzalez, Fluid Phase Equilib. 123 (1996) 167–187.
[39] A. Dahmani, A. Ait Kaci, I. Mokbel, G. Ghanem, J. Jose, J. Chim. Phys. 92 (1995) 1093–1103.
[40] J.M. Prausnitz, Molecular Thermodynamics of Fluid Phase Equilibria, Prentice-Hall, Englewood Cliffs, NJ, 1969.
[41] B.L. Larsen, P. Rasmussen, A. Frendeslund, Ind. Eng. Chem. Res. 26 (1987) 2274–2286.
[42] J. Gmehling, J. Li, M. Schiller, Ind. Eng. Chem. Res. 32 (1993) 178–193.
[43] K. Kniaz, Fluid Phase Equilib. 68 (1991) 35–46.
[44] M. Barbe, D. Patterson, J. Phys. Chem. 82 (1978) 40–45.
[45] M. Barbe, D. Patterson, J. Solution Chem. 9 (1980) 753–769.